



21st European Conference on Fracture, ECF21, 20-24 June 2016, Catania, Italy

Prediction of ductile failure using a phenomenological model calibrated from micromechanical simulations

J.K. Holmen^{a,b,*}, L.E.B. Dæhli^{a,b}, O.S. Hopperstad^{a,b}, T. Børvik^{a,b}

^aStructural Impact Laboratory (SIMLab), Department of Structural Engineering, Norwegian University of Science and Technology (NTNU), NO-7491, Trondheim, Norway

^bCentre for Advanced Structural Analysis (CASA), NTNU, NO-7491, Trondheim, Norway

Abstract

Unit-cell models were in this study utilized to numerically determine the failure locus of a cast and homogenized AA6060 aluminum alloy. Simulations were conducted for moderate and high stress triaxiality ratios, and for various Lode parameters between generalized tension and generalized compression. We estimated the orientation of the localization band that minimizes the failure strain in the unit-cell models for all the imposed stress states. The energy based Cockcroft-Latham (CL) failure criterion was calibrated based on the numerically determined failure locus and used in finite element simulations that we evaluated against experimental tests. Test-specimen geometries included smooth tension tests, notched tension tests and plane strain tension tests. These were designed to cover a wide range of stress states. The points of failure in the experimental tests were predicted with reasonable accuracy by the numerical simulations. We see that the method used for numerically determining the failure locus can be improved by refining the micromechanical simulations. Better agreement between the simulations and the experiments can also be obtained, for instance by employing a different macroscopic failure criterion than the CL criterion.

Copyright © 2016 The Authors. Published by Elsevier B.V. This is an open access article under the CC BY-NC-ND license (<http://creativecommons.org/licenses/by-nc-nd/4.0/>).

Peer-review under responsibility of the Scientific Committee of ECF21.

Keywords: Unit-cell models; Finite element simulations; Ductile failure; Numerical prediction; Experimental validation

1. Introduction

Both the stress triaxiality ratio and the Lode parameter influence material response and the development of damage in metals. Because of this, several material tests are needed to extract enough data to calibrate macroscopic failure criteria for all relevant stress states. Previous works have successfully managed to predict the yield stress and

* Corresponding author. Tel.: +47 93 04 58 37.

E-mail address: jens.k.holmen@ntnu.no

the work hardening of Al-Mg-Si alloys at room temperature without conducting mechanical tests (see e.g. Myhr et al. (2010)). Subsequent studies used a similar procedure to predict the material behavior before finite element analyses were conducted to simulate rather complex structural problems (Johnsen et al. (2013) and Holmen et al. (2015)). A disadvantage of these works was that no information regarding material failure could be determined without conducting experimental tests, so measures were taken to circumvent the need for a failure criterion.

In this paper we propose and test a possible method of applying microstructural modeling to calibrate a macroscopic failure criterion. If this proves successful it means that we can, at least in theory, predict the yielding, work hardening and failure of Al-Mg-Si aluminum alloys with minimal experimental testing. The results presented in this paper are mainly qualitative, and they illustrate the proposed method of predicting failure which is under development and still somewhat immature.

The stress triaxiality ratio T is a measure of the hydrostatic stress state, and the Lode parameter L is a measure of the deviatoric stress state. They are commonly used to categorize material tests. In the following they are defined as

$$T = \frac{I_1}{3\sigma_{\text{eq}}} \quad \text{and} \quad L = \sqrt{3} \tan \theta_L = \frac{2\sigma_2 - \sigma_1 - \sigma_3}{\sigma_1 - \sigma_3} \quad (1)$$

where I_1 is the trace of the stress tensor, σ_{eq} is the equivalent stress, σ_i are the ordered principal stresses and θ_L is the Lode angle defined from the axis of generalized shear.

In this paper we consider the Cockcroft-Latham (CL) failure criterion (Cockcroft and Latham (1968)) that can be expressed as

$$D = \frac{1}{W_{\text{cr}}} \int_0^{p_f} \langle \sigma_1 \rangle dp = \frac{1}{W_{\text{cr}}} \int_0^{p_f} \left\langle T + \frac{3-L}{3\sqrt{3+L^2}} \right\rangle \sigma_{\text{eq}} dp, \quad \langle \sigma_1 \rangle = \max(0, \sigma_1). \quad (2)$$

The criterion is, as seen, implicitly dependent on T and L . D is the damage variable, W_{cr} is the failure parameter of the model, p is the equivalent plastic strain and p_f is the equivalent plastic failure strain.

The procedure we use in this paper is as follows: Micromechanical simulations are used to determine the failure locus for the material at hand. The failure parameter W_{cr} of the CL failure criterion presented above (or the parameters of other failure criteria) is then adjusted to fit the failure locus and subsequently used in finite element simulations.

2. Material

An AA6060 aluminum alloy in a cast and homogenized state was used in this work. The heat treatment process ensured that the plastic flow of the material is almost isotropic. More information about the material processing, and the particle content, microstructure and scanning electron micrographs of fracture surfaces can be found in Westermann et al. (2014) where the same material was presented in detail.

Table 1 presents the material parameters in the extended Voce hardening rule that we use to represent the hardening behavior. These parameters were taken from Westermann et al. (2014) and are based on mechanical tests. It should be noted that these parameters could have been obtained using a nano-scale material model (Johnsen et al. (2013)). The extended Voce hardening rule is a function of the equivalent plastic strain and it reads

$$\sigma_y(p) = \sigma_0 + R(p) = \sigma_0 + \sum_{i=1}^2 Q_i (1 - \exp(-C_i p)), \quad (3)$$

where σ_0 is the initial yield stress while Q_i and C_i are hardening parameters. The non-quadratic Hershey yield criterion (Hershey (1954)) is adopted in the form

$$f(\sigma_1, \sigma_2, \sigma_3, p) = \left(\frac{1}{2} \left(|\sigma_1 - \sigma_2|^a + |\sigma_2 - \sigma_3|^a + |\sigma_3 - \sigma_1|^a \right) \right)^{\frac{1}{a}} - \sigma_y(p) \leq 0, \quad (4)$$

where the exponent a controls the curvature of the yield surface. In this study $a = 8$ was used since aluminum is a face centered cubic material (Logan and Hosford (1980)).

3. Parameter identification

3.1. Unit-cell simulations

Establishing the failure locus of the AA6060 aluminum alloy proved to be rather cumbersome. We did a series of unit-cell simulations under proportional loading for $T = \sqrt{3}/3 \approx 0.577, 1.0, 2.0$ and 3.0 , and $L = -1, 0$ and 1 . For $L = 0$ we also simulated with $T = 0.33$ and 0.0 , meaning that we have 14 points in total. Failure is in the unit-cell simulations defined as the point where the major principal stress reaches its maximum. This was done for several reasons: First, it is relatively straight forward to identify in all the analyses. Second, it is the most conservative assumption, making the predictions safer to use in design. Last, it has been used in similar approaches before; see for instance Tvergaard (1981) and (1982).

The failure strain in the unit-cell simulations is dependent on the angle α (see Fig. 1a), that is the angle between the normal of the band of localization and the direction of the major principal stress. So we ran simulations with five different α to estimate the critical band angle for each combination of T and L (see e.g. Barsoum and Faleskog (2007) and Dunand and Mohr (2014)). Ideally we should have conducted even more analyses in order to determine the critical angle more accurately, but this is outside the scope of this study. The simulations were conducted in a finite element framework using the ABAQUS/Implicit solver (see also Dæhli et al. (2016)). The initial void volume fraction was taken as $f_0 = 0.005$ (Westermann et al. (2014)) and the hardening behavior and yield surface of the matrix material was described by Eq. (3) and (4), respectively. Fig. 2 shows an example of an un-deformed unit cell and the same cell after failure initiation. Based on the 14 points of failure from proportional loading paths and critical localization band angle, we can find a failure locus that is shown with dashed lines in Fig. 1b.

Table 1: Material parameters describing the extended Voce hardening curve.

A (MPa)	Q_1 (MPa)	C_1	Q_2 (MPa)	C_2
66.26	62.00	32.36	126.46	4.21

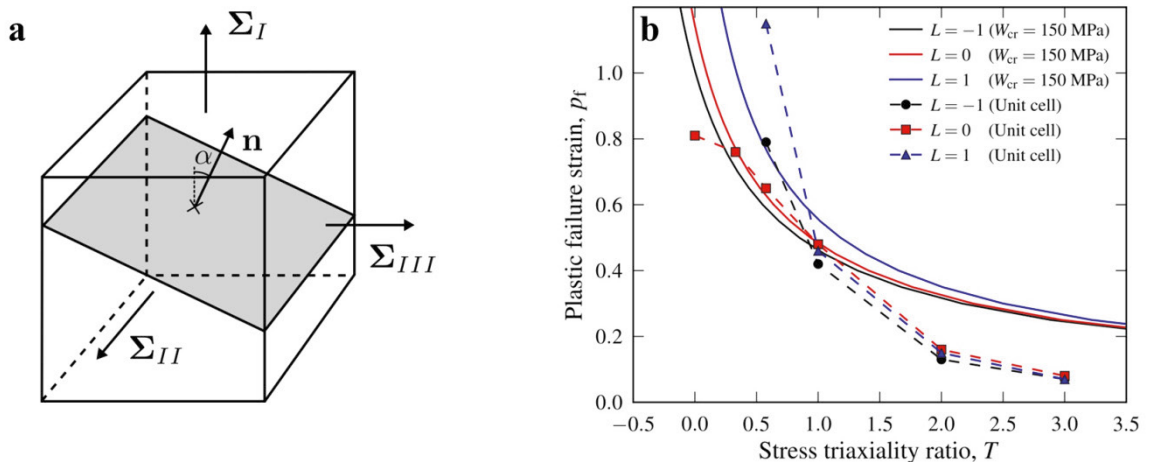


Fig. 1: (a) Illustration of the localization band where $\Sigma_I \geq \Sigma_{II} \geq \Sigma_{III}$ are the ordered macroscopic principal stresses and α is the angle between the Σ_I axis and the band normal \mathbf{n} . (b) Failure locus determined from the unit-cell analyses and the locus described by the CL failure criterion.

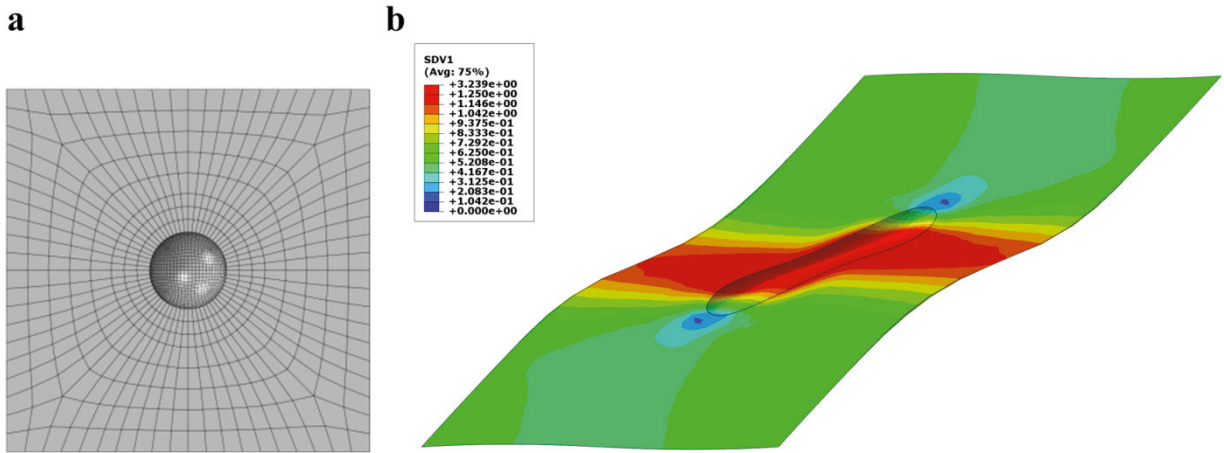


Fig 2: (a) Un-deformed unit cell and (b) deformed unit cell at failure. Fringes represent equivalent plastic strain ($T = 0.577, L = 0.0, \alpha = 44.1^\circ$).

3.2. Identification procedure

We used the failure locus shown in Fig. 1b to identify the parameter in the CL failure criterion. Given a specific material, W_{cr} is the only parameter that is required to define the CL failure surface. For $D = 1$ we can plug Eq. (3) into Eq. (2) and obtain an expression for T as a function of L and p :

$$T = \frac{W_{cr}}{\sigma_0 p_f + \sum_{i=1}^2 \left(Q_i p_f + \frac{Q_i}{C_i} ((\exp(-C_i p_f) - 1)) \right)} - \frac{3-L}{3\sqrt{3+L^2}} \tag{5}$$

It is now possible to minimize the difference between Eq. (5) and the failure locus from unit-cell simulations to obtain an estimate of W_{cr} . Fig. 1b shows how the CL failure criterion with the CL parameter that gives the best fit, $W_{cr} = 150$ MPa, compared to the results from the unit-cell simulations. It is clear that a better fit can be obtained with another failure criterion. For instance the failure criterion of Johnson and Cook (1985), which is based on the analysis by Rice and Tracey (1969), would adhere better to the predicted failure locus, but it is in its original form not dependent upon the Lode parameter.

4. Evaluation of the procedure

4.1. Experiments

The following experimental tests were used to evaluate the failure parameter that we identified in Section 3: uniaxial axisymmetric tension tests (UT), notched axisymmetric tension tests (NT), and plane strain tension tests (PST). Their geometries are shown in Fig. 3. The UT and NT tests were conducted by Westermann et al. (2014). Two notch radii were used in the notched tests – giving four different combinations of T and L as seen in Table 2. According to the definition of the Lode parameter given in Eq. (1), generalized tension is represented by $L = -1$ and generalized shear is represented by $L = 0$. The initial stress triaxiality ratios were found with Bridgman’s analysis.

All the axisymmetric tension tests (UT and NT) were stretched with a cross-head velocity of 1.2 mm/min corresponding to an initial strain rate of 5.0×10^{-4} for the smooth specimens. Two perpendicular lasers measured the reduction in area all the way to fracture of the specimens while a calibrated load cell monitored the force level. Fig. 4a shows the true stress-strain curves.

For the plane strain tension tests (PST) the force was measured by a calibrated load cell and the displacement of the actuator was measured by the test-machine. Additional 3D digital image correlation (3D-DIC) analysis was used to extract the displacement and strain fields from the 10 mm gauge area, and these measurements confirmed the plane strain assumption. Fig. 4b shows the force-elongation curves from the tests. Here, the elongation was taken from a virtual extensometer in the DIC analysis. As specified in Fig. 4b the length of this virtual extensometer varied between 5 and 6 mm depending on the test.

4.2. Macroscopic simulations

We made finite element simulation models in ABAQUS/Explicit based upon the geometries shown in Fig. 3. For the axisymmetric UT and NT tests we employed four-node axisymmetric quadrilateral elements (CAX4R) while we used 8-node linear brick elements (C3D8R) for the PST test. Reduced integration and hourglass control was used in both cases. Time scaling was used to reduce the computational time, and the kinetic energy was checked and found to be negligible in all analyses.

Fig. 4a shows the numerical simulations compared to corresponding axisymmetric tension tests. The strength level is adequately captured and the failure strains are overestimated or underestimated depending on the test specimen geometry. The point of failure is underestimated in the UT test. For the NT test with $R = 2.0$ mm the point of failure is overestimated, this is common when using the CL criterion. As seen in Fig. 1b, the correspondence between unit-cell simulations and the CL criterion is poorest at high stress triaxiality ratios. The simulation of the NT test with $R = 0.8$ mm predicts the point of failure almost perfectly. We believe that this is because the experimental tests were more ductile than expected. This is supported by the fact that the failure strain for $R = 0.8$ mm is almost the same as the failure strain for $R = 2.0$ mm in the tests.

By comparing the simulation to the experiments of the PST tests (Fig. 4b) we see that the strength is overestimated by almost 10 % even though we use the Hershey yield surface. The Hershey yield surface significantly decreases the strength level in plane strain tests compared to a von Mises yield surface, but apparently not enough in this case. Further, failure happened prematurely in the simulation of this specimen geometry.

Table 2: Initial stress state in the material tests

Specimen type	UT	NT ($R = 2.0$ mm)	NT ($R = 0.8$ mm)	PST
Stress triaxiality ratio (T)	0.33	0.893	1.389	0.577
Lode parameter (L)	-1	-1	-1	0

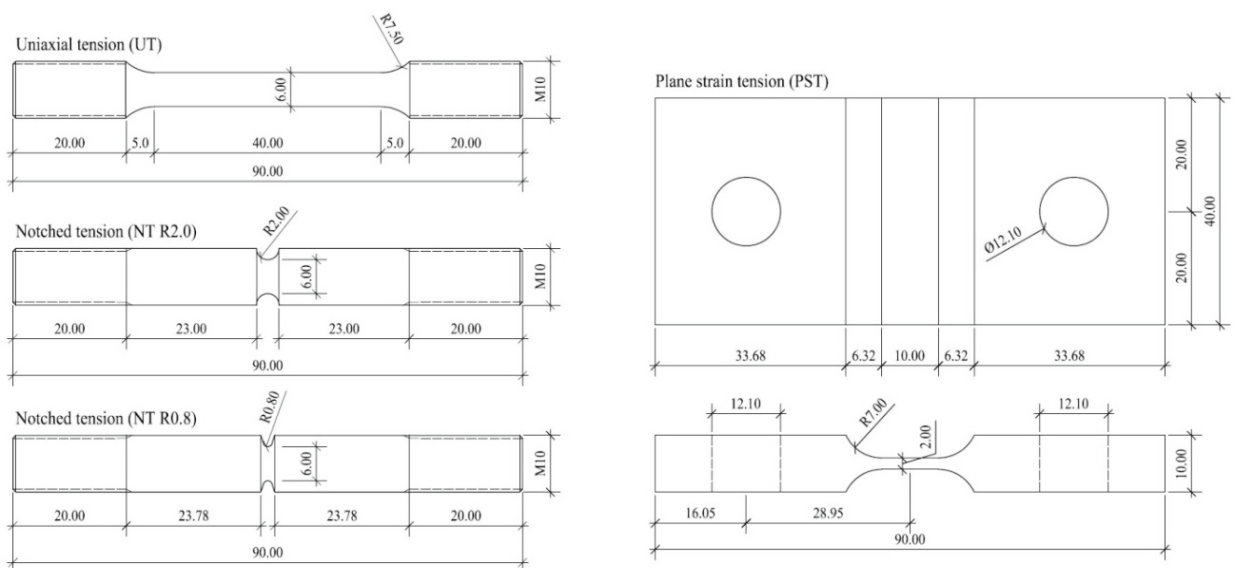


Fig. 3: Specimen geometries used in the experimental and numerical evaluation of the parameters, all measurements are in mm.

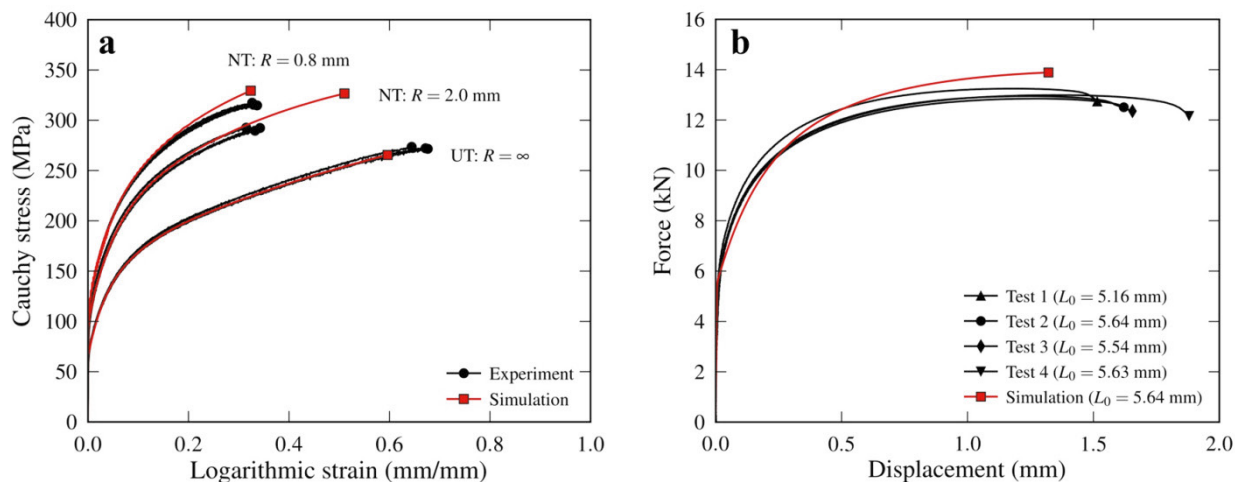


Fig. 4: Results from the macroscopic numerical simulations and corresponding experiments. (a) Stress-strain curves from the axisymmetric tension (UT and NT) tests, (b) force-elongation curves from the plane strain (PST) tension test.

5. Concluding remarks

In this paper we illustrated a method of calibrating a model for ductile failure from numerical simulations. We found that the Cockcroft-Latham (CL) failure criterion calibrated from unit-cell simulations predicted the point of failure in the evaluation experiments with reasonable accuracy. This specific performance of the CL criterion was not, however, the main objective of this paper. Instead we tried to focus on the procedure and to highlight its possibilities and disadvantages.

The biggest weakness of the results presented here is that we have assumed an initial void volume fraction in the unit-cell simulations, meaning that the approach is not completely uncoupled from experimental test data. Further, to improve the results we need to consider additional combinations of the Lode parameter and stress triaxiality ratio to get a more accurate failure locus. More angles α (that is, the angle between the normal of the localization band and the direction of the major principal stress) should also be investigated. Although the initial idea for this paper was to obtain results from low stress triaxiality ratios by using a particle in the unit-cell simulations we encountered several problems when attempting to simulate this and explicit finite element analysis is most likely needed to improve the contact definition.

What we observe from the best fit to the failure locus is that the CL criterion is not capable of capturing the failure strain over the entire range of stress triaxiality ratios. So a different failure criterion should be adopted in future work. Another method of generating a failure locus is to perform a set of bifurcation or imperfection analyses where the angle of the localization band that gives the critical failure strain can be determined. It does appear that a more refined micromechanical model and a more flexible macroscopic failure criterion need to be employed in subsequent works.

The work presented in this paper is still somewhat immature and there are many conceivable changes and improvements that can be made. Still, a method similar to this might in the future make it possible to predict yielding, work hardening and failure of aluminum alloys based on the chemical composition and thermo-mechanical processing route of the material, and a minimum of mechanical tests.

Acknowledgements

This research was supported by the Structural Impact Laboratory (SIMLab) at the Norwegian University of Science and Technology. The authors would also like to thank the Research Council of Norway for support through the Centre for Advanced Structural Analysis (CASA).

References

- Barsoum, I., Faleskog, J., 2007. Rupture mechanisms in combined tension and shear – Micromechanics. *International Journal of Solids and Structures* 44, 5481 – 5498.
- Cockcroft, M.G., Latham, D.J., 1968. Ductility and the workability of metals. *Journal of the Institute of Metals* 96, 33–39.
- Dunand, M., Mohr, D., 2014. Effect of Lode parameter on plastic flow localization after proportional loading at low stress triaxialities. *Journal of the Mechanics and Physics of Solids* 66, 133–153.
- Dæhli, L.E.B., Børvik, T., Hopperstad, O.S., 2016. Influence of loading path on ductile fracture of tensile specimens made from aluminium alloys. *International Journal of Solids and Structures* (<http://doi:10.1016/j.ijsolstr.2016.03.028>).
- Hershey, A.V., 1954. The plasticity of an isotropic aggregate of anisotropic face centered cubic crystals. *Journal of Applied Mechanics* 21, 241–249.
- Holmen, J.K., Børvik, T., Myhr, O.R., Fjær, H.G., Hopperstad, O.S., 2015. Perforation of welded aluminum components: Microstructure-based modeling and experimental validation. *International Journal of Impact Engineering* 84, 96–107.
- Johnsen, J., Holmen, J.K., Myhr, O.R., Hopperstad, O.S., Børvik, T., 2013. A nano-scale material model applied in finite element analysis of aluminium plates under impact loading. *Computational Materials Science* 79, 724–735.
- Johnson, G.R., Cook, W.H., 1985. Fracture characteristics of three metals subjected to various strains, strain rates, temperatures and pressures. *Engineering Fracture Mechanics* 21, 31–48.
- Logan, R.W., Hosford, W.F., 1980. Upper-bound anisotropic yield locus calculations assuming $\langle 111 \rangle$ -pencil glide. *International Journal of Mechanical Sciences* 22, 419–430.
- Myhr, O.R., Grong, Ø., Pedersen, K.O., 2010. A combined precipitation, yield strength and work hardening model for Al-Mg-Si alloys. *Metallurgical and Materials Transactions* 41A, 2276–2289.
- Rice, J.R., Tracey, D.M., 1969. On the ductile enlargement of voids in triaxial stress fields. *Journal of the Mechanics and Physics of Solids* 31, 1–24.
- Tvergaard, V., 1981. Influence of voids on shear band instabilities under plane strain conditions. *International Journal of Fracture* 17, 389–407.
- Tvergaard, V., 1982. On localization in ductile materials containing spherical voids. *International Journal of Fracture* 18, 237–252.
- Westermann, I., Pedersen, K.O., Furu, T., Børvik, T., Hopperstad, O.S., 2014. Effects of particles and solutes on strength, work hardening and ductile fracture of aluminium alloys. *Mechanics of Materials* 79, 58–72.